buildings

MDPI

Article

Study on Seismic Response and Parameter Influence in a Transformer–Bushing with Inerter Isolation System

Ruoyu Zhang [1], Meigen Cao [2,*] and Jizhong Huang [3]

[1] School of Mechanics and Engineering Science, Shanghai University, Shanghai 200444, China; 21820359@shu.edu.cn
[2] School of Civil Engineering, North China University of Technology, Beijing 100144, China
[3] Institute for Conservation of Cultural Heritage, Shanghai University, Shanghai 200444, China; hjizhong@163.com
* Correspondence: caomeigen@ncut.edu.cn

Abstract: In this paper, a mechanical model of a transformer–bushing with an inerter isolation system (IIS) is established. An IIS is composed of an inerter element, a damping element, and a spring element connected in parallel between the same two terminals. Vibration control equations and frequency response functions are also established. The influence of parameters on IIS, including inerter–mass ratio, damping ratio, and frequency ratio, was studied. In the extremum condition that represents the most efficient parameter set of inerter–mass ratio and damping ratio for relative displacement response ratio, an optimal design method was developed by exploiting a performance demand. Finally, the seismic response of the transformer–bushing with IIS was carried out to verify the isolation performance of IIS. The research shows that the equivalent mass coefficient and damping coefficient of IIS can be amplified by an inerter element and the inerter–mass ratio and damping ratio are reduced simultaneously under the conditions of meeting the performance demand after parameter optimization. Meanwhile, the parameter optimization design method proved to be effective for meeting the target demand of the relative displacement response of the bushing and tank, while base shear force and isolation displacement were reduced simultaneously. Based on the results from a response history analysis under ground motion records, IISs can significantly suppress the resonance response of a structure and the continuous vibration response in the stable state. The peak displacement can be reduced by 50% compared with a traditional isolation system.

Keywords: transformer–bushing system; inerter element; isolation system; stochastic response; parameter optimization; seismic response

Citation: Zhang, R.; Cao, M.; Huang, J. Study on Seismic Response and Parameter Influence in a Transformer–Bushing with Inerter Isolation System. *Buildings* **2022**, *12*, 530. https://doi.org/10.3390/buildings12050530

Academic Editor: Jia-Bao Yan

Received: 26 March 2022
Accepted: 15 April 2022
Published: 22 April 2022

1. Introduction

Lifeline structures have high vulnerability under earthquakes [1], such as transformer–bushing systems [2]. The main reason is that the natural vibration frequency of the structure is close to the predominant frequency of external excitation [3], resulting in the amplification of vibration response [4]; therefore, vibration mitigation and control in the structure is particularly important. Many researchers have noticed that isolation technology can effectively reduce the base shear force at the bottom of the transformer and reduce the displacement response of tank, bushing and auxiliary facilities [5], so as to protect the transformer from various disasters in strong earthquakes. Fujita et al. [6,7] carried out a test analysis of laminated rubber isolation bearings for transformers and other large gravity equipment, focusing on the development of isolation devices and verifying vibration control effect, without considering the interaction between transformers and bushings. Thu Pham [8] carried out a shaking table test of transformer–bushing. During the test, a vibration isolation device composed of steel cable was installed between the transformer frame and bushing, and a viscous damping system was set under the transformer frame to transformer oil. The test showed that the vibration isolation device has the vibration

isolation effect of significantly reducing the acceleration response at the top of the bushing. Murota et al. [9–11] designed three types of isolation systems at the bottom of the transformer model: BS isolation, the friction pendulum system (FPS), and the segmented combined high–damping rubber isolation system (SHRB). To verify the effectiveness of the above three types of isolation systems, shaking table tests were carried out and the numerical models of base isolation system and SHRB isolation system were established, after which theoretical analysis and research were carried out. However, the displacement of the isolation layer of the traditional isolation measures was large, and the vibration control effect of the upper bushing with large height was not satisfactory. Hence, it is necessary to develop an isolation system that can control the vibration response of bushing and isolation layer simultaneously. An inerter isolation system (IIS) for seismic response mitigation of transformer–bushings is proposed in this paper.

In the last ten years, the electromechanical similarity theory [12] has provided a theoretical basis for the proposal of an inerter element, and the vibration mitigation and isolation technology based on inerter element has been developed. Compared with the traditional tuned mass damper (TMD), a damper with an inerter element can directly and effectively control inertial force at two terminals. Moreover, the inerter element can effectively enlarge the small actual mass through methods such as ball screw to convert the translational motion into rotary motion. In 2001, Smith [13,14] put forward the concept of an inerter element based on electromechanical similarity theory, described the basic forms of a ball screw inerter element and a rack and pinion inerter element; later designing a hydraulic inerter element in 2013 [15] that has a simpler structure and greater robustness. Subsequently, shock absorbers based on different inerter element connection forms were developed, such as the tuned viscous mass damper (TVMD) with a mass element in parallel with damping element, and the tuned inerter damper (TID) with a stiffness element in parallel with damping element. At the same time, the design method of inerter systems has also been studied. Ikago et al. [16] derived a simple formula for TVMD optimization design based on fixed–point theory. Pan et al. [17] studied the parameters of single–degree–of–freedom structures with different inerter systems considering the natural damping of the original structure and the output cost control of the damper, made up for deficiencies in design method based on the fixed–point theory, and proposed the SPIS–II inerter damping system design method [18]. Hwang et al. [19] proposed a ball screw inerter system connected with a toggle brace. Through theoretical analysis and numerical calculation, it is shown that the system can be effectively used in a structure even when the drift is very small. Zhang et al. [20,21] applied the inerter damper system to high–rise structures such as chimneys and wind power towers, conducted theoretical analysis and parameter influence analysis and proved the effectiveness of the inerter damping system in high–rise structures. Gao et al. [22] put forward an optimum design procedure of VID based on the output feedback control theory for controlling specific cable mode vibrations. While some Japanese scholars have used the inerter damping support in practical engineering [23], most of the research on the inerter damping system is still in the stage of theoretical analysis and numerical simulation. Only the simplified mechanical model is used for the damping analysis of various structures, and only a few scholars have proposed the connection mode and design method for inerter systems applied in building structures [24]. Xie et al. [25,26] put forward a cable–bracing inerter system (CBIS), which is composed of cable and an inerter energy–dissipation system fixed at the bottom of the interlayer of a structure. Parameter analysis and optimization design were carried out and showed that it is easy to install and can effectively control structural displacement. Wang et al. [27] put forward a new tuned inerter negative–stiffness damper (TINSD) for seismic protection of structures, which is more effective than the TID, TVMD, and INSD in reducing the dynamic response of structures. Zhang et al. [28,29] have proposed a hybrid isolation system by employing the recently developed inerter element for seismic response mitigation of a storage tank, in terms of sloshing height, base shear force, and isolation displacement.

In this paper, an inerter isolation system (IIS) for transformer–bushings is proposed. The IIS is composed of an inerter element, a damping element, and a spring element connected in parallel between the same two terminals. First, Section 2 introduces the basic principle of IIS; the equivalent mass and equivalent damping of the isolation layer are improved. In Section 3, the motion control equations and frequency response functions of transformer–bushings with IIS are established. In Section 4, the parameter analysis and parameter optimization is carried out to obtain the minimum inerter–mass ratio and damping ratio of IIS under the condition of meeting the performance demand. Finally, the dynamic response analyses of transformer–bushings with IIS under the ground motion are carried out in Section 5 to verify the vibration control effect of IIS; the mechanism of vibration mitigation of inerter element in the IIS is explained in terms of displacement mitigation and energy dissipation in detail. The research in this paper can provide reference for the design of efficient and lightweight isolation vibration mitigation schemes of transformer–bushing systems based on an inerter system.

2. Theoretical Analysis of Transformer–Bushing with Inerter Isolation Systems

2.1. Mechanical Model of Inerter Element and IIS

Compared with the mass unit, the inertia unit can increase inertia by rotating. The two ends of the unit have different accelerations, and its output is also directly proportional to the relative acceleration at both ends, which can be expressed as:

$$f_I = m_d(a_2 - a_1) \tag{1}$$

where, f_I is the output force of the inerter unit, a_1 and a_2 are the accelerations at both ends, and Figure 1a is the mechanical model of the inerter element. The inerter element is the same as the mass element and cannot dissipate energy by itself. It is generally used in combination with the damper. For example, it forms an inerter isolation system (IIS) in parallel with the damper and spring at the bottom of the structure. IIS obtains greater damping and equivalent mass through the amplification of the inerter and does not increase the apparent volume and mass of the system itself, so as to realize the lightweight of the isolation control system. The mechanical model is shown in Figure 1b.

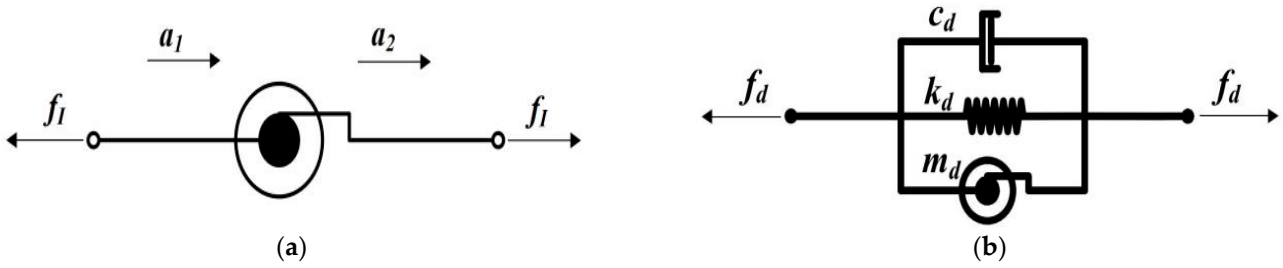

Figure 1. Mechanical model: (**a**) an inerter element; (**b**) IIS.

2.2. Mechanical Model of Transformer–Bushing System with IIS

The transformer–bushing system is generally composed of the main body of the transformer and the upper bushings. The main body of the transformer is composed of a tank, conservator, radiator, stiffener, and other components, and the upper bushings system is composed of an elevated seat, porcelain bushings or composite bushings, grading ring, and other components. The center of gravity of the tank of the transformer is lower, and the mass is much larger than that of the bushings. Therefore, when simplifying the transformer–bushing system, the lower tank, conservator radiator, and other structures can be simplified as a single mass point without considering the deformation of the wall of the tank, which is considered to undergo rigid body motion during earthquakes; the bushing is flexible, the stiffness is smaller, and the center of gravity is high, so the relative displacement between the bushing and the tank should be considered. Figure 2 shows the transformer–bushing system and isolation layer, where h_t and h_b are the height of the center

of gravity of the tank and the center of gravity of the bushing from the ground, respectively.

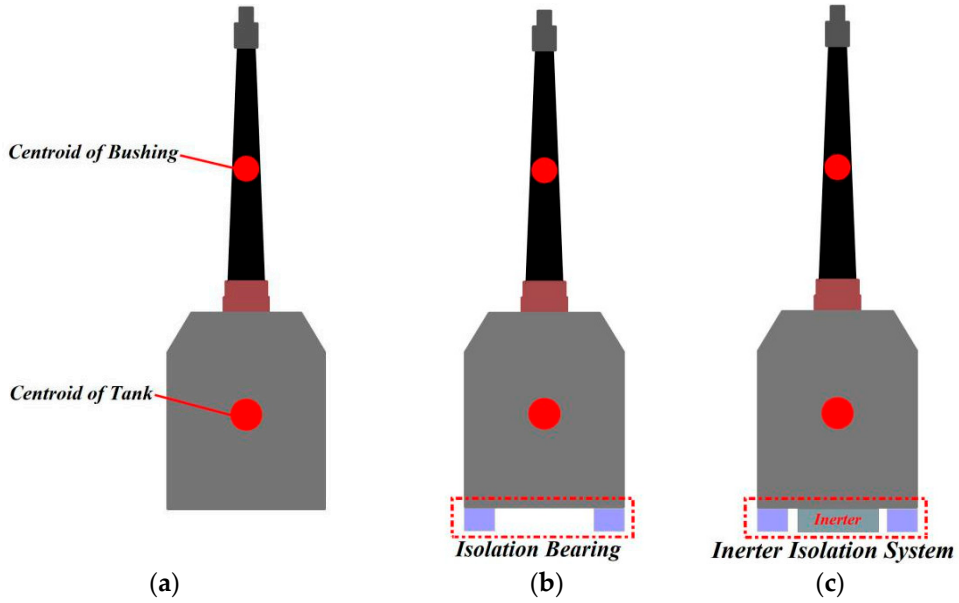

Figure 2. Transformer–bushing system and isolation layer: (**a**) original; (**b**) IB; (**c**) IIS.

For traditional isolation systems [30,31], the isolation bearings, e.g., elastomeric [32] or wire rope isolators [33], are installed at the bottom of the transformer–bushing system. The mechanical model of the bearing can be simplified as the parallel connection of the stiffness element and damping element, which is called the isolation bearing (IB) in this paper. For the inerter isolation system, an additional inerter is added on the isolation bearings. Figure 3 shows the mechanical model of the transformer–bushing system with IIS and IB installed. Where m_t, m_b, and b are the mass of the tank, bushing, and the equivalent mass of inerter, respectively, c_{eq} and c_b are the damping coefficient of isolation bearing and bushing respectively, and k_{eq} and k_b are the stiffness of isolation bearing and bushing, respectively.

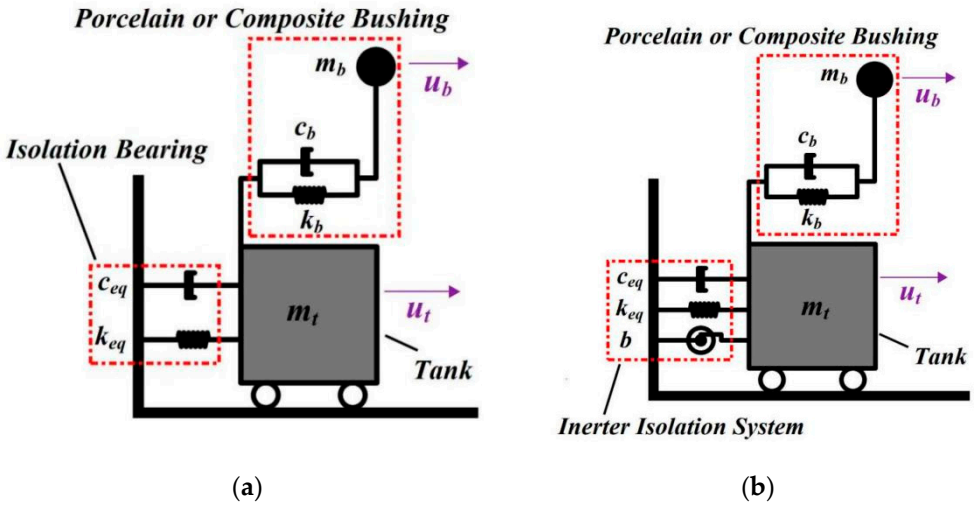

Figure 3. Mechanical model of transformer–bushing system: (**a**) IB; (**b**) IIS.2.3. Motion Control Equation of Transformer–Bushing System with IIS.

According to the mechanical model shown in Figure 3, if the axial displacements of the isolation base are neglected at the same time, the motion equations of two particles of the transformer–bushing system are established:

$$M\ddot{X} + C\dot{X} + KX = -M_0 a_g \tag{2}$$

where: $\ddot{X}, \dot{X}, X$ is the acceleration, velocity, and displacement vector of each mass of the transformer–bushing system, and a_g is the acceleration under seismic action; M, C, and K are the mass, damping, and stiffness matrix of the isolation system respectively, and M_0 is the mass matrix of the transformer–bushing system without isolation.

When considering the isolation bearings installed, as in the case of traditional base–isolated buildings [34] or rigid blocks [35], the M, C, K and motion vectors can be expressed as:

$$M = M_0 = \begin{bmatrix} m_t & \\ & m_b \end{bmatrix}, C = \begin{bmatrix} c_{eq} + c_b & -c_b \\ -c_b & c_b \end{bmatrix}, K = \begin{bmatrix} k_{eq} + k_b & -k_b \\ -k_b & k_b \end{bmatrix} \tag{3}$$

$$X = \begin{Bmatrix} u_{t,IB} \\ u_{b,IB} \end{Bmatrix}, \dot{X} = \begin{Bmatrix} \dot{u}_{t,IB} \\ \dot{u}_{b,IB} \end{Bmatrix}, \ddot{X} = \begin{Bmatrix} \ddot{u}_{t,IB} \\ \ddot{u}_{b,IB} \end{Bmatrix} \tag{4}$$

when considering the inerter isolation system installed, where M_0, C and K are the same as the isolation bearings system, the mass matrix M and the vectors displacement, velocity and acceleration can be expressed as:

$$M = \begin{bmatrix} m_t + b & \\ & m_b \end{bmatrix}, X = \begin{Bmatrix} u_{t,IIS} \\ u_{b,IIS} \end{Bmatrix}, \dot{X} = \begin{Bmatrix} \dot{u}_{t,IIS} \\ \dot{u}_{b,IIS} \end{Bmatrix}, \ddot{X} = \begin{Bmatrix} \ddot{u}_{t,IIS} \\ \ddot{u}_{b,IIS} \end{Bmatrix} \tag{5}$$

where: u_t and u_b are displacement vectors of tank and bushing, IB and IIS are inerter isolation system and isolation bearing.

For the convenience of parameter analysis, the following dimensionless parameters are defined. The parameters of isolation layer and bushing are shown in Equations (6) and (7) respectively. Where μ is the inerter–mass ratio, κ is the frequency ratio of isolation layer and bushing, ζ_{eq} is the damping ratio of the isolation layer, ζ_b is the damping ratio of bushing; ω_b is the circlar frequency of bushing, μ_b is the mass ratio of bushing and tank, ω_{eq} is the circular frequency of the isolation layer.

$$\zeta_{eq} = \frac{c_{eq}}{2m_t\omega_{eq}}, \omega_{eq} = \sqrt{\frac{k_{eq}}{m_t}}, \kappa = \frac{\omega_{eq}}{\omega_b}, \mu = \frac{b}{m_t} \tag{6}$$

$$\zeta_b = \frac{c_b}{2m_b\omega_b}, \omega_b = \sqrt{\frac{k_b}{m_b}}, \mu_b = \frac{m_b}{m_t} \tag{7}$$

Simultaneous solving of Equations (3)–(7) and Laplace transformation of Equation (2) can obtain the motion Equations (8) and (9) of the transformer–bushing system with isolation bearing and inerter isolation system in frequency domain respectively:

$$\begin{bmatrix} 1 & \\ & 1 \end{bmatrix} \begin{Bmatrix} s^2U_{t,IB} \\ s^2U_{b,IB} \end{Bmatrix} + \begin{bmatrix} 2\omega_b(\kappa\zeta_{eq} + \mu_b\zeta_b) & -2\mu_b\omega_b\zeta_b \\ -2\omega_b\zeta_b & 2\omega_b\zeta_b \end{bmatrix} \begin{Bmatrix} sU_{t,IB} \\ sU_{b,IB} \end{Bmatrix} + \begin{bmatrix} \omega_b^2(\kappa^2 + \mu_b) & -\mu_b\omega_b^2 \\ -\omega_b^2 & \omega_b^2 \end{bmatrix} \begin{Bmatrix} U_{t,IB} \\ U_{b,IB} \end{Bmatrix} = \begin{Bmatrix} -1 \\ -1 \end{Bmatrix} A_g \tag{8}$$

$$\begin{bmatrix} 1+\mu & \\ & 1 \end{bmatrix} \begin{Bmatrix} s^2U_{t,IIS} \\ s^2U_{b,IIS} \end{Bmatrix} + \begin{bmatrix} 2\omega_b(\kappa\zeta_{eq} + \mu_b\zeta_b) & -2\mu_b\omega_b\zeta_b \\ -2\omega_b\zeta_b & 2\omega_b\zeta_b \end{bmatrix} \begin{Bmatrix} sU_{t,IIS} \\ sU_{b,IIS} \end{Bmatrix} + \begin{bmatrix} \omega_b^2(\kappa^2 + \mu_b) & -\mu_b\omega_b^2 \\ -\omega_b^2 & \omega_b^2 \end{bmatrix} \begin{Bmatrix} U_{t,IIS} \\ U_{b,IIS} \end{Bmatrix} = \begin{Bmatrix} -1 \\ -1 \end{Bmatrix} A_g \tag{9}$$

where s is the Laplace operator, $s = i\Omega$, Ω is the ground motion excitation frequency, and $U_{t,IB}$, $U_{b,IB}$, $U_{t,IIS}$, $U_{b,IIS}$, and A_g are the Laplace transform of $u_{t,IB}$, $u_{b,IB}$, $u_{t,IIS}$, $u_{b,IIS}$, and a_g, respectively. From the linear matrix equations of Equations (8) and (9), $U_{t,IB}$, $U_{b,IB}$, $U_{t,IIS}$, and $U_{b,IIS}$ can be respectively solved. At the same time, the displacement response transfer

functions of the bushing and tank with IB ($H_{Ub,IB}(s)$, $H_{Ut,IB}(s)$) and IIS ($H_{Ub,IIS}(s)$, $H_{Ut,IIS}(s)$) can be obtained as follows:

$$\begin{cases} H_{U_{t,IB}}(s) = \frac{U_{t,IB}(s)}{A_g(s)}, H_{U_{b,IB}}(s) = \frac{U_{b,IB}(s)}{A_g(s)} \\ H_{U_{t,IIS}}(s) = \frac{U_{t,IIS}(s)}{A_g(s)}, H_{U_{b,IIS}}(s) = \frac{U_{b,IIS}(s)}{A_g(s)} \end{cases} \tag{10}$$

3. Parameter Analysis of IIS

According to Parseval's Theorem, the root mean square (RMS) response σ of the system excited by white noise is obtained as follows:

$$\sigma = \int_0^T \frac{u^2(t)}{T_0} dt = \sqrt{\int_{-\infty}^{+\infty} |H(i\Omega)|^2 S_0 d\Omega} \tag{11}$$

where S_0 is the power spectrum of white noise. Therefore, the effect of the isolation system can be measured by comparing the reduction rate of the root mean square response of relative displacement of the bushing and the isolation layer with and without an isolation system. For the transformer–bushing system with IB and IIS installed, the displacement mitigation ratio of bushing $\gamma_{U,IB}$ and $\gamma_{U,IIS}$ is:

$$\gamma_{U,IB}(\omega_b, \zeta_{eq}, \kappa) = \frac{\left|\sigma_{U_{b,IB}} - \sigma_{U_{t,IB}}\right|}{\sigma_{U_{b,0}}}, \gamma_{U,IIS}(\omega_b, \zeta_{eq}, \kappa, \mu) = \frac{\left|\sigma_{U_{b,IIS}} - \sigma_{U_{t,IIS}}\right|}{\sigma_{U_{b,0}}} \tag{12}$$

where $\sigma_{Ub,0}$ is the root mean square response of the displacement of the original bushing. At the same time, the ratio of the root mean square of relative displacement response after base isolation can be calculated to compare the isolation effects of the two isolation systems; secondly, the ratio of the root mean square of displacement response of the isolation layer of IIS and IB can be calculated to reflect the stability of the isolation layer of the two isolation systems; finally, the ratio of root mean square of base shear force response of IIS and IB can be calculated to reflect the force output of the isolation layer. For a transformer–bushing structure with IB and IIS installed, the relative displacement response ratio of the two isolation systems γ_U, the displacement response ratio of isolation layer γ_{ID}, and base shear force response ratio γ_{SF} are in the Formula (13), where σ_{SF} is the root mean square of base shear force response of the transformer–bushing system.

$$\gamma_U(\omega_b, \kappa, \zeta_{eq}, \mu) = \frac{\gamma_{U,IIS}}{\gamma_{U,IB}}, \gamma_{ID}(\omega_b, \zeta_{eq}, \kappa, \mu) = \frac{\sigma_{U_{t,IIS}}}{\sigma_{U_{t,IB}}}, \gamma_{SF}(\omega_b, \zeta_{eq}, \kappa, \mu) = \frac{\sigma_{SF,IIS}}{\sigma_{SF,IB}} \tag{13}$$

At the same time, it is also necessary to analyze the interaction between the bushing and the tank. Assuming that the stiffness coefficient and damping ratio of transformer–bushing are constants, then μ_b can reflect the relationship between the flexibility and mass of the bushing. The greater the μ_b, the higher the height of the bushing and the greater the flexibility. This is used to describe bushings with high center of gravity and low engineering frequency (1–3 Hz). The smaller the μ_b, the smaller the height and the greater the stiffness of the bushing. This is used to describe bushings with low center of gravity and high engineering frequency (3–10 Hz). The predominant frequency of ground motion is between 1–10 Hz, so the size of value of engineering frequency of the bushing is relative to the seismic action. Table 1 shows the parameters of bushings with different engineering frequencies, where LB represents bushings with low frequency, HB represents bushings with high frequency, and f_b is the engineering frequency of the transformer–bushing.

Table 1. Parameters of bushings.

Parameters of Bushing	*Low Frequency Bushing*		*High Frequency Bushing*	
	LB–1	***LB–2***	***HB–1***	***HB–2***
μ_b	0.060	0.220	0.005	0.020
$h(m)$	5.0	10.0	1.2	2.5
$f_b(Hz)$	2.1	1.2	7.1	3.5

Parameter analysis of isolation layer select inerter–mass ratio μ, frequency ratio κ and damping ratio ζ_{eq}. The index of parameter analysis is the relative displacement response ratio of bushing γ_U, displacement ratio of isolation layer γ_{ID}, and base shear force response ratio γ_{SF}. The parameter range of inerter–mass ratio μ in parameter analysis is [0.01,10], frequency ratio κ, and damping ratio ζ_{eq} is [0.01,1].

3.1. Relative Displacement Response Ratio γ_U

The relative displacement between the bushing and tank can directly reflect the seismic response level of the bushing, and it is also the most important index in the vibration control of the transformer–bushing system. Therefore, the relative displacement of the bushing should be taken as the primary control index, and the random vibration analysis of the transformer–bushing isolation system under white noise input should be carried out. First, the inerter–mass ratio μ is analyzed. When the inerter–mass ratio is fixed, the influence of inerter–mass ratio on the isolation layer can be seen directly. Figure 4 shows the relative displacement response ratio γ_U when changing the damping ratio ζ_{eq} with different types of bushing systems.

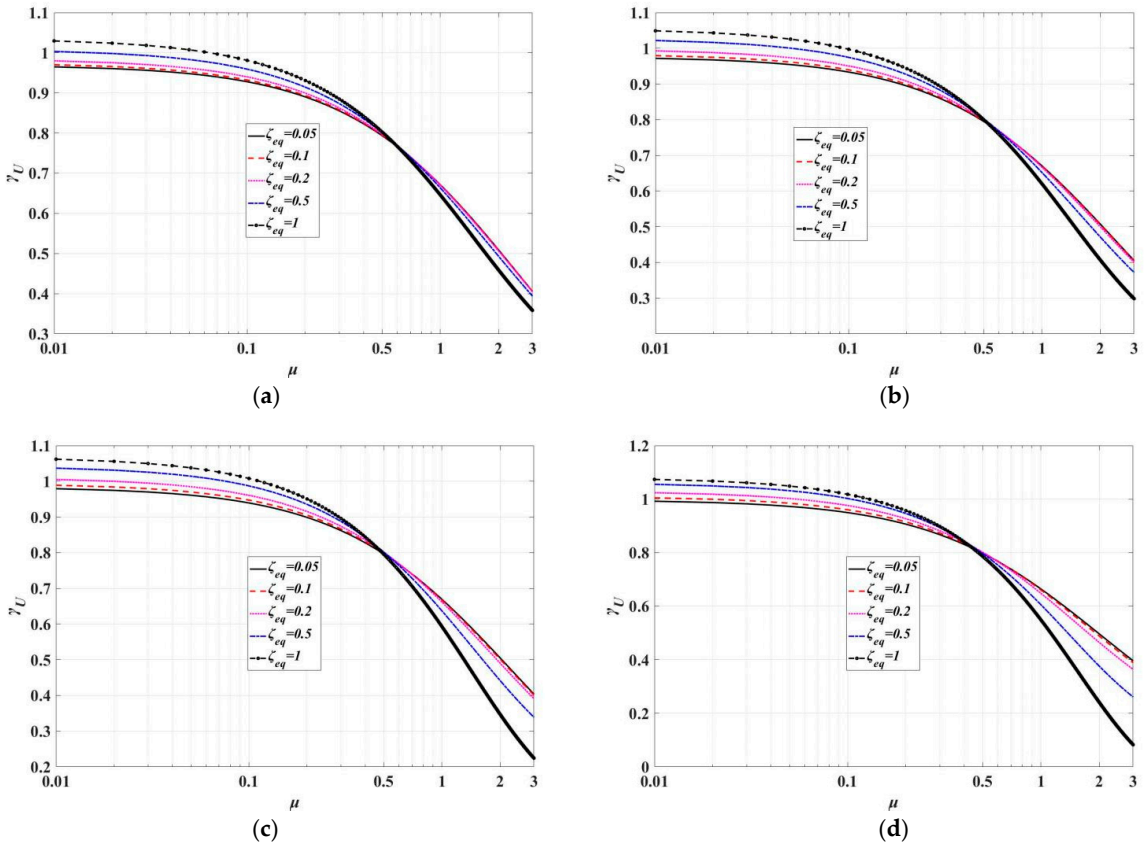

Figure 4. Curves of γ_U under different damping ratio ζ_{eq} (κ = 0.1, ζ_b = 0.02): (**a**) *HB–1*; (**b**) *HB–2*; (**c**) *LB–1*; (**d**) *LB–2*.

In the isolation design, the frequency ratio of the isolation layer should not be too large, so κ = 0.1 is a fixed value for analysis. The variety of bushings with different frequencies with inerter–mass ratio is the same, γ_U decreases with the increase of inerter–mass ratio, and the greater the damping ratio of isolation layer, the greater the reduction of γ_U in larger value of μ. The influence of the inerter–mass ratio on low–frequency bushings is more obvious. When the inerter–mass ratio is greater than 0.5, the decline of γ_U becomes faster. When the inerter–mass ratio is between [1,2], the RMS of relative displacement response of bushings with IIS is about 0.5 times of those with IB, and the displacement control effect of the inerter element is better. If the inerter–mass ratio continues to increase, we will see yet lower values of γ_U. However, cost will greatly increase, and the increase of inerter–mass ratio will also increase the base shear force of the isolation layer. Considering that the linear IB system has satisfactory isolation effects on the transformer–bushing system, the target γ_U can be set between 0.5–0.7, so inerter–mass ratio is between [0.5,2].

Second, the frequency ratio of isolation layer of IIS is considered. The inerter–mass ratio is taken as 0.5, 1, and 2, respectively, and the damping ratio of isolation layer ζ_{eq} is 0.1, 0.5, and 1. The influence of frequency ratio on γ_U is shown in Figure 5. The γ_U of bushings with different frequencies is almost a fixed value when it is within [0.001,0.05], which is less affected by the frequency ratio. When κ is [0.1,1], it decreases first and then increases significantly; the greater the inerter–mass ratio and damping ratio, the greater the influence of the frequency ratio. For bushings with high frequency, the stability range of γ_U is κ is equal to [0.001,0.1]; for bushings with low frequency, the stability range of γ_U is κ is equal to [0.001,0.0.5]. Hence, to ensure the robustness of the isolation layer of IIS on the displacement control of the upper bushing, the value of κ should not be greater than 0.1.

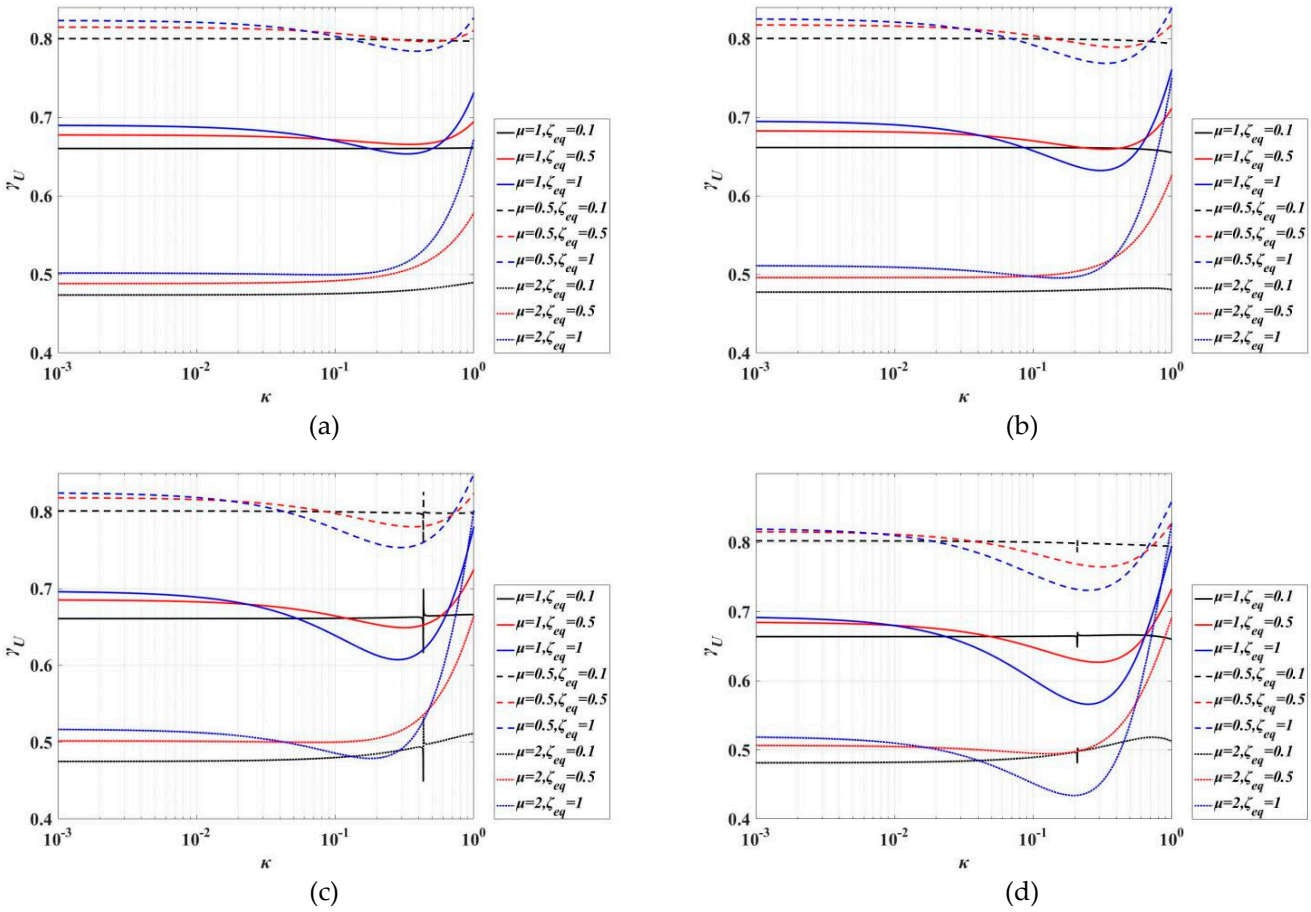

Figure 5. Curves of γ_U: (**a**) *HB–1*; (**b**) *HB–2*; (**c**) *LB–1*; (**d**) *LB–2*.

3.2. Displacement Response Ratio of Isolation Layer γ_{ID}

The smaller the relative displacement between the bushing and the tank, the more that the response of the tank and the bushing tends towards being the same, but excessive displacement of the isolation layer can easily cause overturning of the superstructure. Therefore, the displacement of the isolation layer is also an index that can not be ignored in vibration control of the transformer–bushing system. As the displacement of the isolation layer in a normal IB system is large, the displacement response ratio γ_{ID} of the isolation layer can be used in the analysis as an index to seek the trend of each parameter. Figures 6–9 show displacement response ratios of isolation layer γ_{ID} under different frequency ratios κ of four different types of transformer–bushing systems.

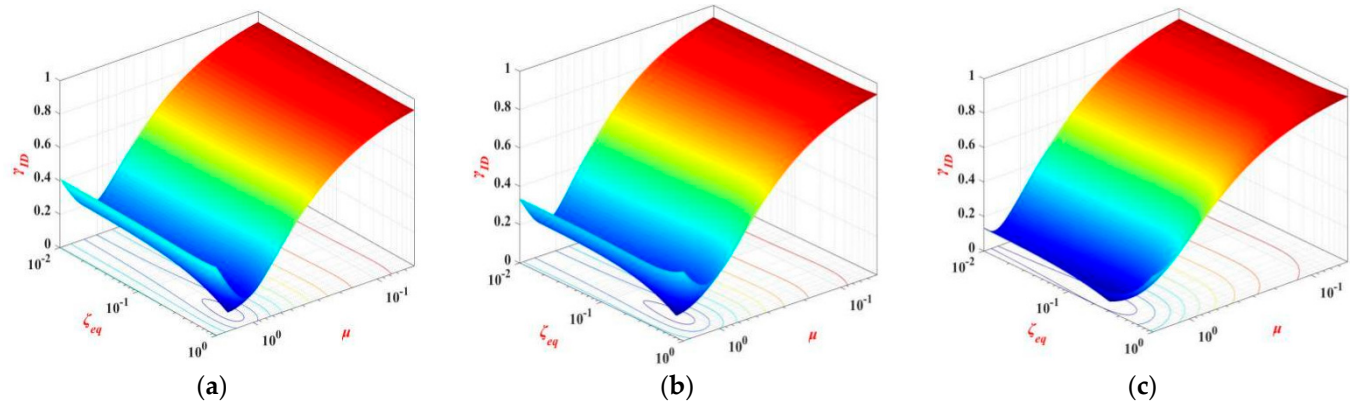

Figure 6. Contour plot of γ_U of *HB–1*: (**a**) κ = 0.05; (**b**) κ = 0.1; (**c**) κ = 0.3.

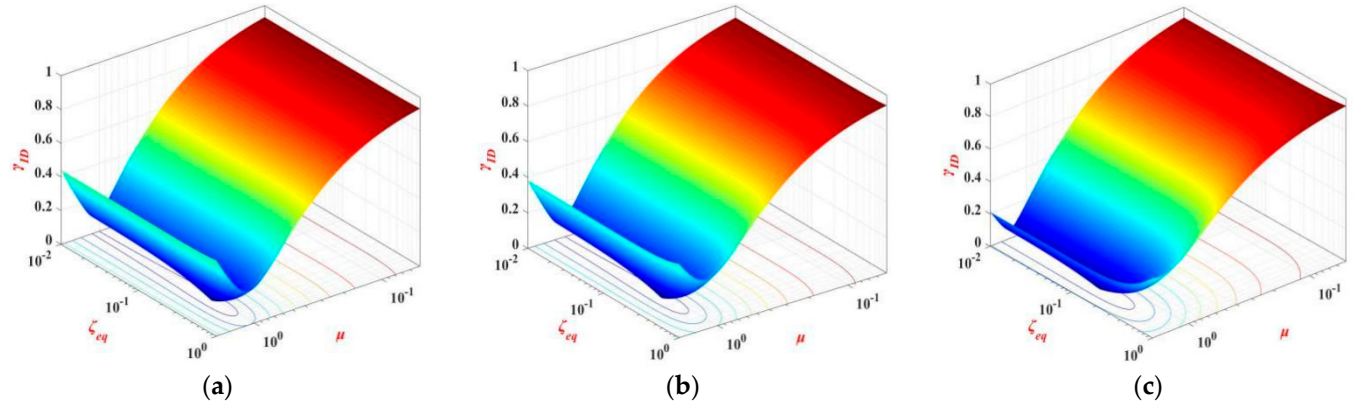

Figure 7. Contour plot of γ_U of *HB–2*: (**a**) κ = 0.05; (**b**) κ = 0.1; (**c**) κ = 0.3.

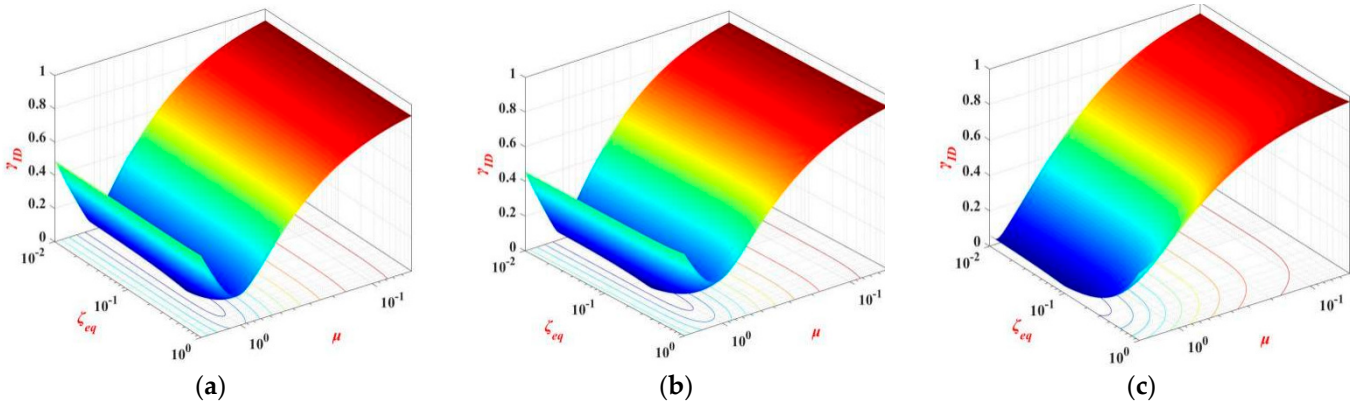

Figure 8. Contour plot of γ_U of *LB–1*: (**a**) κ = 0.05; (**b**) κ = 0.1; (**c**) κ = 0.3.

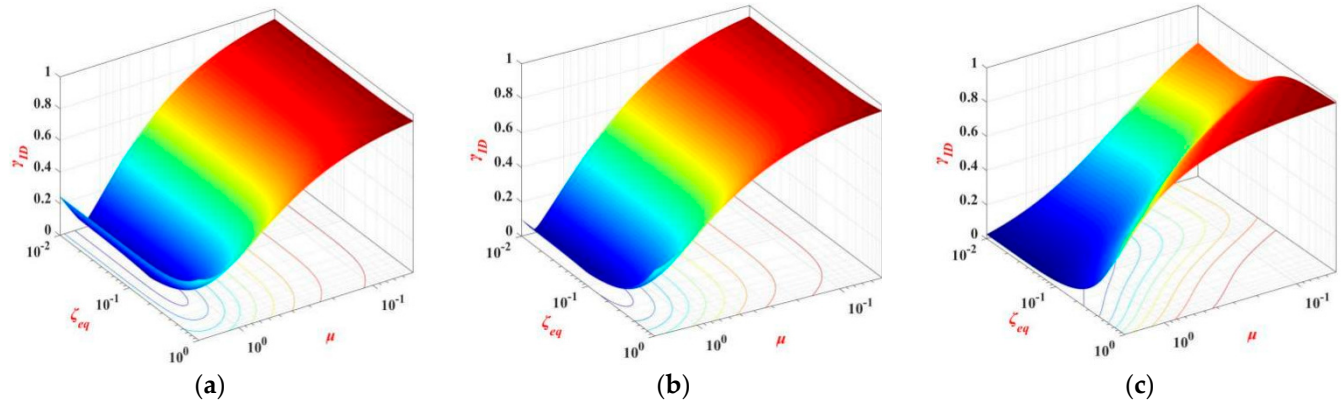

Figure 9. Contour plot of γ_U of *LB–2*: (**a**) κ = 0.05; (**b**) κ = 0.1; (**c**) κ = 0.3.

The γ_{ID} is the ratio of the displacement ratios of the isolation layer of the two isolation systems, so the damping ratio has little effect. Only low–frequency bushings (LB–2) show large fluctuation at κ = 0.3. However, γ_{ID} is greatly affected by the inerter–mass ratio, and like γ_U, will decrease with the increase of inerter–mass ratio within a certain range. However, when the inerter–mass ratio is between [1,2], the four kinds of bushing γ_{ID} will increase with the increase of the inerter–mass ratio. The smaller the frequency ratio is, the more flexible the isolation layer is, and the more 'steep' the surface of γ_{ID} is when the inerter–mass ratio is between [1,2], indicating that the restoring force of the isolation layer can not quickly mitigate the additional inertia force generated by the inerter element. Although increasing the stiffness can reduce this phenomenon, the excessive stiffness of thesolationn layer will increase the displacement of the upper bushing. So, when the value of κ is not greater than 0.1, we should try to increase it as much as possible to meet the displacement demands of the isolation layer. As can be seen from Figures 6–9, when the γ_{ID} is greater than 0.4, the demands for the values of various parameters of the isolation layer are low, and the surface of γ_{ID} is stable. At the same time, the damping ratio ζ_{eq} should not be too large. For bushings with low frequency, increasing the damping ratio will increase the displacement of isolation layer. When ζ_{eq} is less than 0.2, the surface of γ_{ID} is relatively stable and robust. The displacement index of isolation layer γ_{ID} is determined to be about 0.4. Meanwhile, when meeting the demands of the displacement mitigation of the isolation layer, the values of various parameters shall be reduced as much as possible.

3.3. Base Shear Force Response Ratio γ_{SF}

The base shear force ratio γ_{SF} is also an important index of the isolation system. We can use it to seek the trend of each parameter and compare it with the trend of displacement index to comprehensively select the final isolation layer parameters. Figures 10–13 show the base shear force ratio of four types of transformer–bushing systems under different frequency ratios κ.

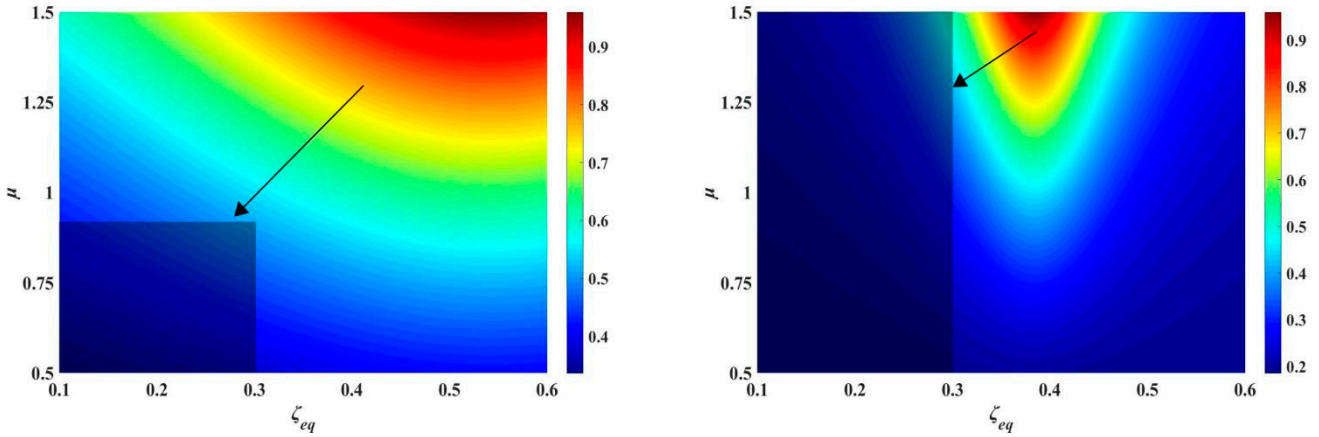

Figure 10. Contour plot of γ_{SF} of *HB–1*: (**a**) κ = 0.05; (**b**) κ = 0.1.

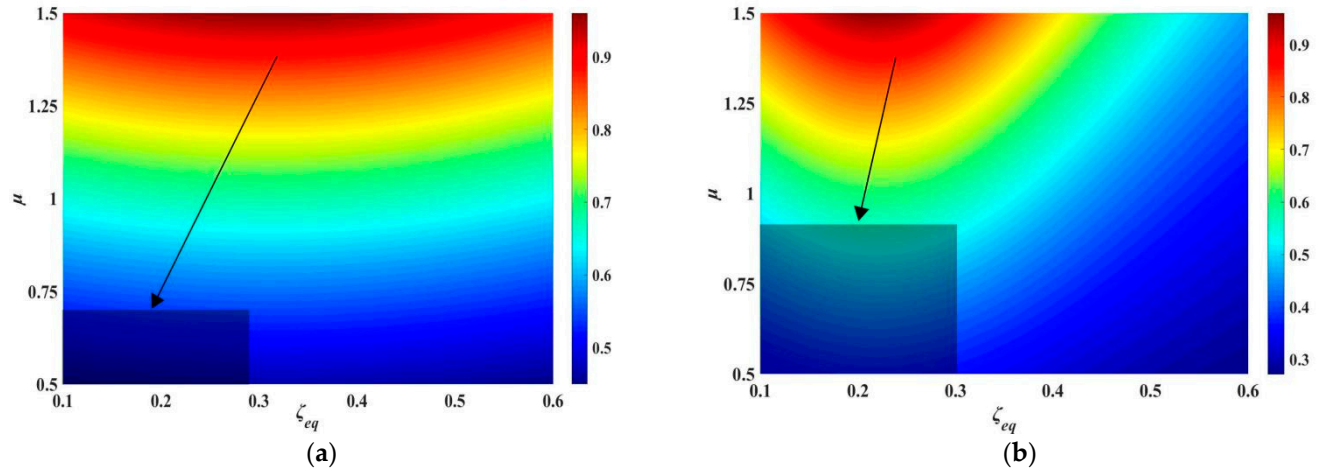

Figure 11. Contour plot of γ_{SF} of *HB–2*: (**a**) κ = 0.05; (**b**) κ = 0.1.

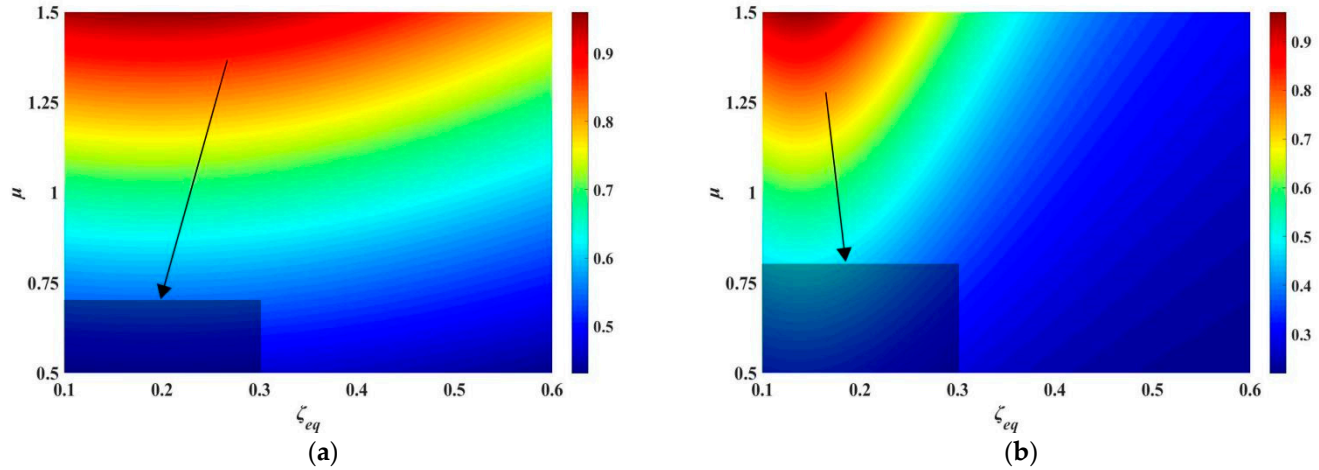

Figure 12. Contour plot of γ_{SF} of *LB–1*: (**a**) κ = 0.05; (**b**) κ = 0.1.

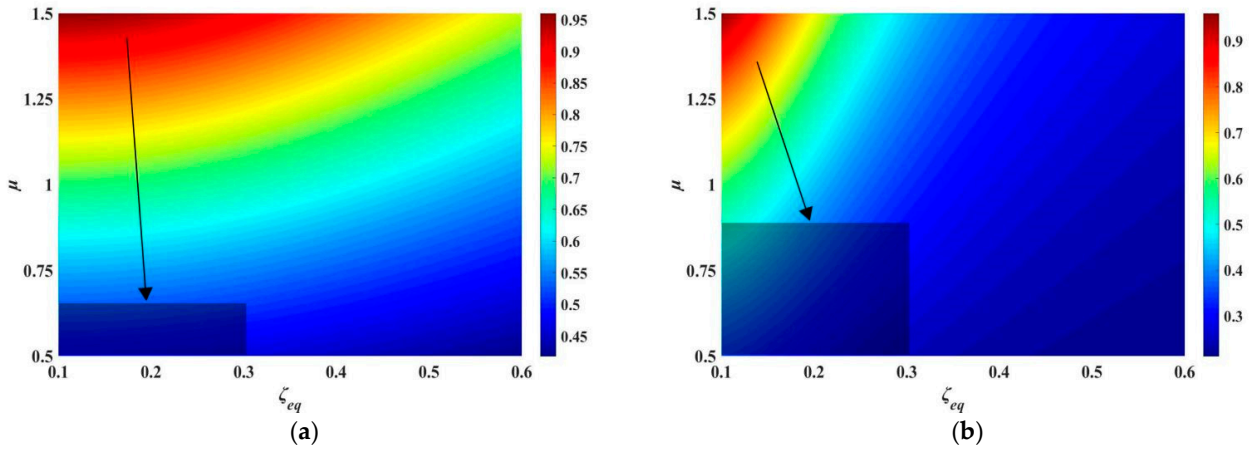

Figure 13. Contour plot of γ_{SF} of *LB–2*: (**a**) κ = 0.05; (**b**) κ = 0.1.

The base shear force of the tank of the IIS is lower than IB when the inerter–mass ratio is within [0.5,1.5], but when the inerter–mass ratio is greater than 1.5, the base shear force of IB is less than IIS, indicating that the large inertance coefficient will increase the force output of the isolation layer. This trend is opposite to γ_U and γ_{ID}. Therefore, under the condition of meeting the displacement index (γ_U and γ_{ID}), the inerter–mass ratio should be reduced as much as possible to reduce the base shear force.

Fix γ_{SF} = 0.5 and the damping ratio is less than 0.5 as the target area in Figures 10–14 (rectangular shadow). It can be seen that when the frequency ratio is 0.05, the target area is smaller and the corresponding optional parameter range becomes smaller for both bushings with low frequency and bushings with high frequency; when the frequency ratio increases to 0.1, the target area increases significantly, and the range of selectable reasonable inerter–mass ratios also expands. At the same time, it can also be seen that the target area of bushings with high frequency is larger than bushings with low frequency, so the bushings with high–frequency difficulty provide easier control over base shear force.

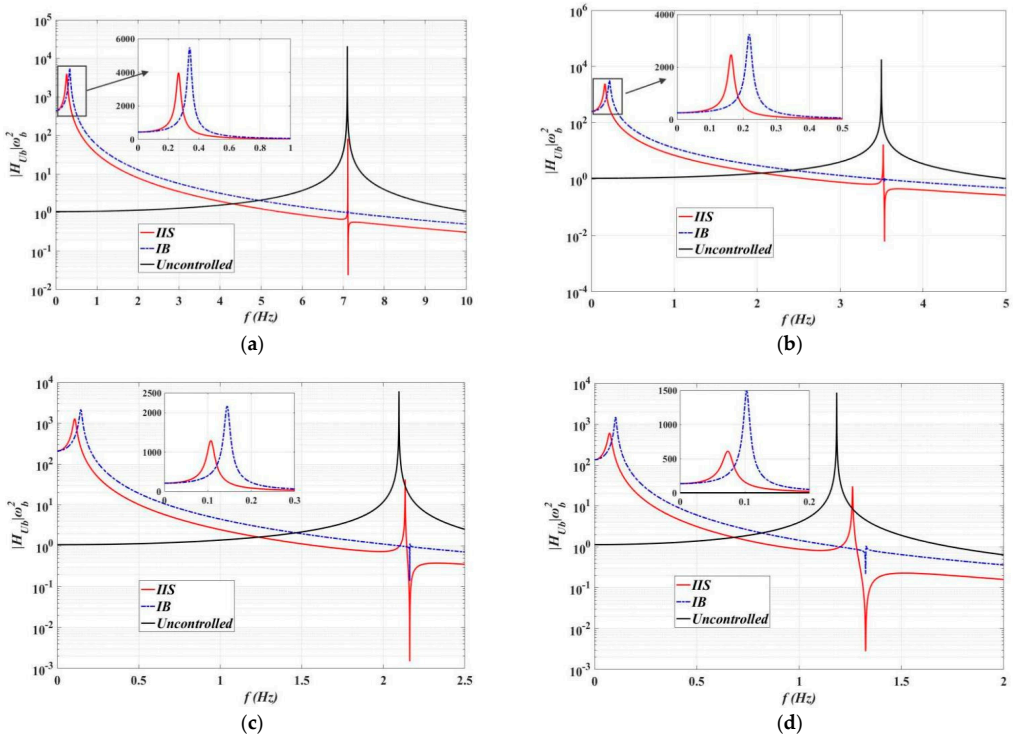

Figure 14. Displacement amplification factor of bushings: (**a**) *HB–1*; (**b**) *HB–2*; (**c**) *LB–1*; (**d**) *LB–2*.

For bushings with high frequency, the inerter–mass ratio can be reduced as much as possible because the amplitude of base shear force is low and the target area is large; due to the fact that the displacement index of bushings with low frequency are more stringent than the base shear force index, the displacement index of bushings with low frequency can be considered first when a larger base shear force ratio is fixed.

3.4. Parameters Optimization Design of IIS

The variation trend of the parameters of the displacement index (γ_U and γ_{ID}) is opposite to that of the base shear force index (γ_{SF}), which is mainly reflected in the damping ratio ζ_{eq} and inerter–mass ratio μ. The determination of IIS parameters is preferentially suggested to be based on the specified extent of vibration mitigation effect in terms of the relative displacement of transformer and bushing γ_U, which is essential to performance. Following the parametric analysis results, in the case of given κ, large μ will lead to larger shear force (shown in Figure 13), and small μ and ξ_{eq} will lead to larger displacement of bushing (shown in Figure 5). We need to obtain a balanced parameter combination in the IIS to mitigate all three indexes.

Hence, the overall design idea of IIS for transformer–bushing isolation control is to meet the demands of bushing relative displacement first, and then consider the displacement of the isolation layer and base shear force. At this point, γ_{ID} and γ_{SF} are considered as additional performance indexes; the relative displacement index is considered first. We can fix the target relative displacement response ratio γ_U according to the performance demands of the transformer–bushing system, and optimize the parameters with extremum conditions [30], that is:

$$\gamma_U(\zeta_{eq}, \kappa, \mu) = \gamma_{U,t} \tag{14}$$

$$\frac{\partial \gamma_U(\zeta_{eq}, \kappa, \mu)}{\partial \mu} = 0, \frac{\partial \gamma_U(\zeta_{eq}, \kappa, \mu)}{\partial \zeta_{eq}} = 0 \tag{15}$$

where $\gamma_{U,T}$ is the target of the relative displacement response ratio. The constraint condition of Equation (15) is to meet the relative displacement response ratio and makes the damping ratio and inerter–mass ratio as small as possible to meet the engineering needs at the same time. This optimization method is concerned with controlling both the performance of the relative displacement of the transformer and bushing γ_U and base shear force γ_{SF}, so that the excessive shear force can be reduced while simultaneously achieving a desired relative displacement mitigation ratio γ_U.

4. Seismic Response

Parameter analysis in the frequency domain was carried out under white noise excitation; to further verify the isolation effect of IIS, a dynamic response analysis of the transformer–bushing system with IIS under non–stationary ground motion was carried out as well. Different values of isolation indexes were selected for four types of bushings, and the optimization parameters were selected according to the optimization method of Equation (14). The best parameters of the isolation layer were selected for time history analysis. The values of the IIS design parameters and optimization indexes of different types of transformer–bushing systems are shown in Table 2. The primary optimization principle is that the bushing with lower frequency should keep a smaller value of γ_U. This reflects the greater control over relative displacement afforded by highly flexible bushings.

Table 2. Results of parameters of IIS obtained after optimization.

	Parameters	***LB–1***	***LB–2***	***HB–1***	***HB–2***
Tank	m_t**(kg)**	10.0×10^4	15.0×10^4	5.0×10^4	7.5×10^4
Bushing	μ_b	0.060	0.220	0.005	0.020
	h**(m)**	5.00	10.00	1.20	2.50
	f_b**(Hz)**	2.10	1.20	7.10	3.50
IIS	μ	0.854	1.056	0.618	0.791
	κ	0.071	0.095	0.048	0.063
	ζ_{eq}	0.113	0.171	0.055	0.070
Primary index	γ_U	0.600	0.500	0.700	0.650
Additional index	γ_{ID}	0.461	0.353	0.621	0.588
	γ_{SF}	0.452	0.598	0.275	0.364

Figure 14 shows the displacement amplification factors of bushings corresponding to Table 2. It can be seen that the natural frequency of the isolation system bushing is reduced, and the displacement responses are also decreased. Compared with the IB system, the displacement amplification factor of IIS is lower, and the response of bushings with low frequency (LB–2) decreases the most. The natural period of the bushing with IIS is further extended, far away from the predominant period of ground motion. At the same time, as the isolation effect of IIS is more obvious, the bandwidth of bushing response after isolation also increases. Figure 15 shows four types of transformer–bushing systems corresponding to Table 2. Similar to the trend in Figure 14, compared with IB system, the amplitudes of transfer function of the base shear force of IIS are lower, and the shear force response of bushing with low frequency is reduced the most.

El Centro wave, Taft wave, Chi Chi wave, and Kobe wave were selected as seismic waves; the predominant frequencies of the four seismic records were different. Figure 16 shows the acceleration response spectra of the four seismic waves. The higher the structural height and weight of the bushing, the higher the seismic vulnerability, and the difficulty of vibration control will increase. Therefore, this paper selects the LB–2 transformer–bushing system, which is the most vulnerable to earthquakes, as the analysis object for analyzing the dynamic time history under four kinds of ground motion inputs. Figure 17 shows the relative displacement time history of the bushing and the transformer, which can reflect the seismic response of the bushing itself; Figure 18 shows the **hysteresis loops** of the isolation layer, which can reflect the displacement response of the isolation layer and the energy dissipation capacity of dampers of IB and IIS.

It can be seen from Figure 17 that the control effect of IB isolation system on the bushing was considerable, and the maximum relative displacement of the bushing can be controlled between 30–50% of the original structure. IIS has a better isolation control effect on the bushing than IB, which is only about 50% of the displacement controlled by IB. The displacement response level is reduced at the same time, and the time history curve is smoother and steadier. It indicates that the overall sloshing speed of the tank and bushing is also reduced.

It can be seen from Figure 18 that IIS has smaller displacement of the isolation layer than IB, and the peak displacement is about 45–60% of IB. Based on the relative displacement response of the bushing in Figure 17, IIS can reduce the displacement of the tank and bushing at the same time and complete the overall isolation control of the transformer–bushing system. At the same time, while reducing the displacement of the isolation layer, the damping element of IIS has a larger hysteresis loop due to the amplification of the inerter element. Compared with IB, the damping force is larger and the energy dissipation effect is amplified.

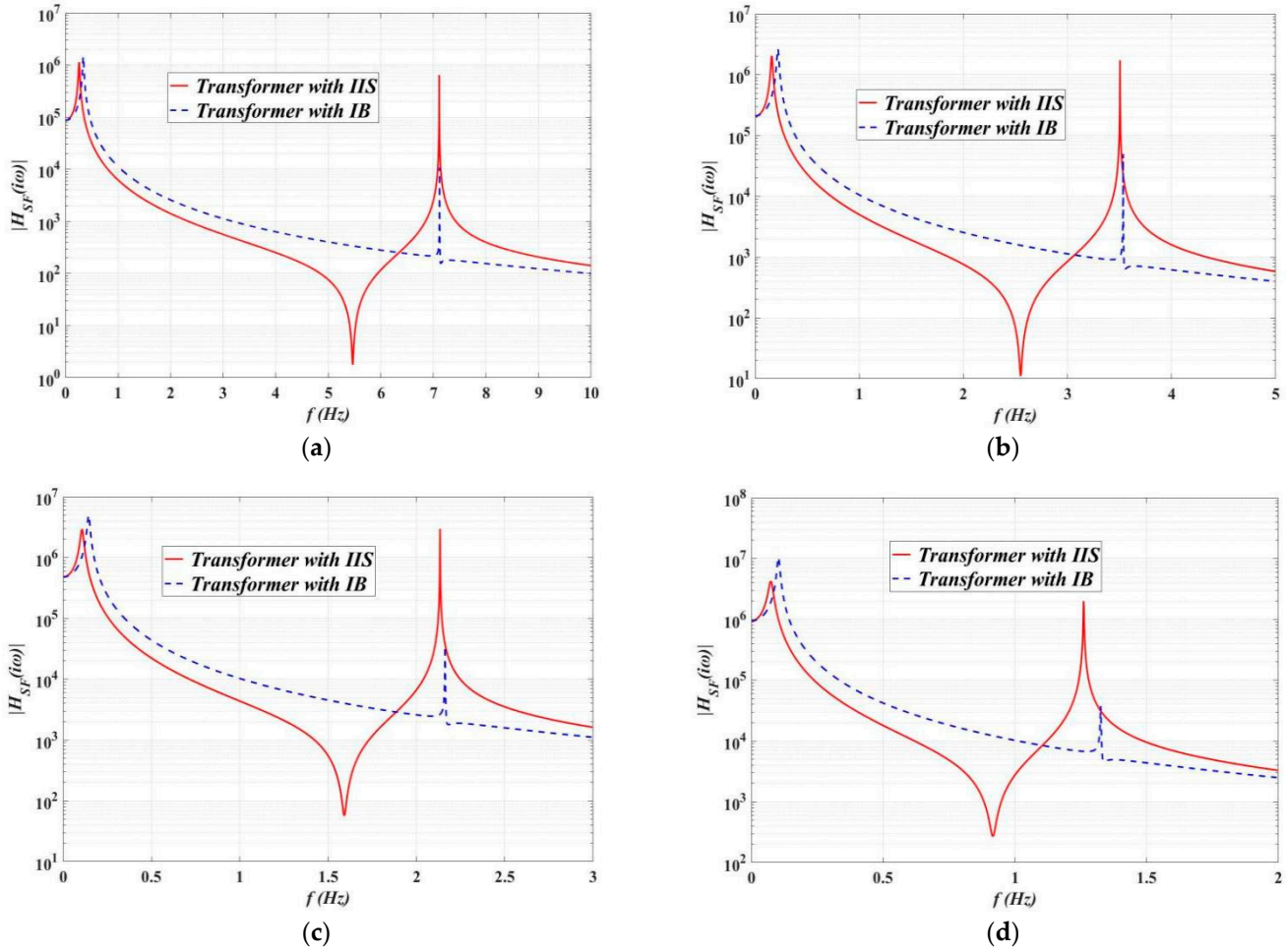

Figure 15. Transfer function curves of base shear force: (**a**) *HB–1*; (**b**) *HB–2*; (**c**) *LB–1*; (**d**) *LB–2*.

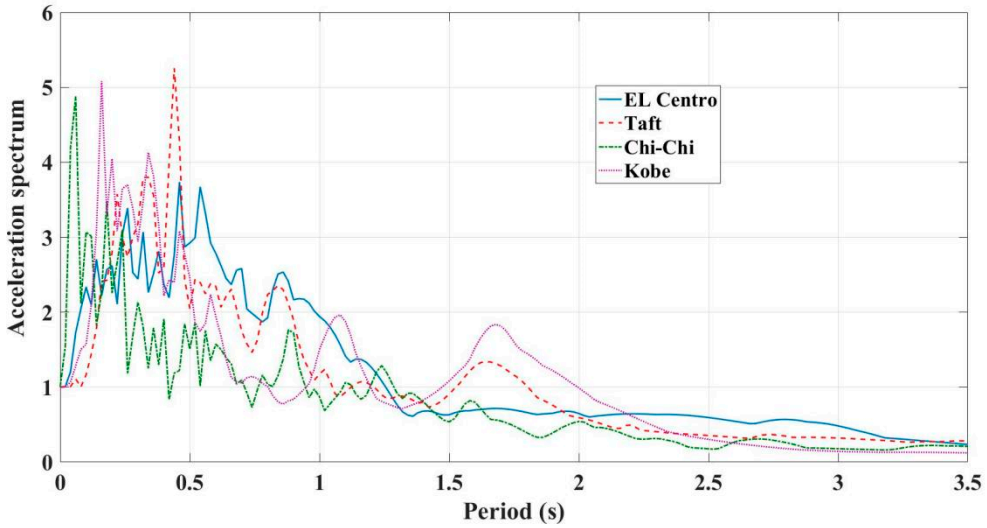

Figure 16. Normalized acceleration spectra of earthquake records.

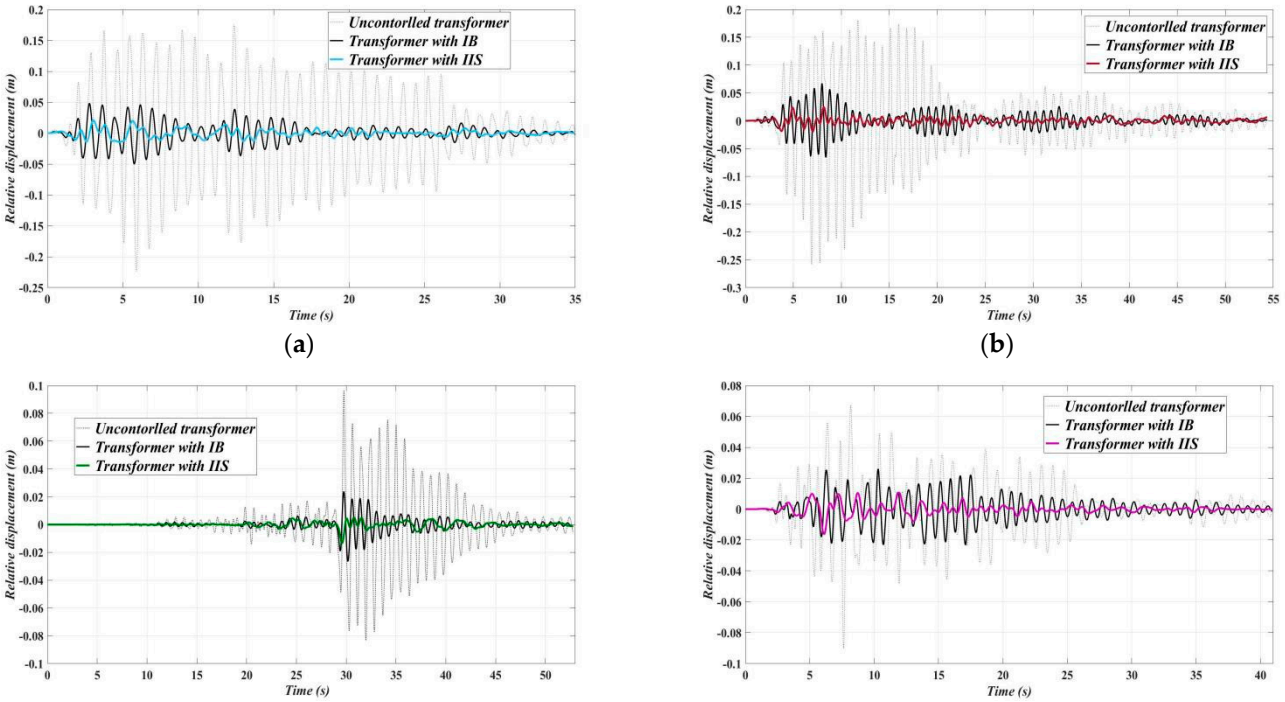

Figure 17. Relative displacement responses of bushing (LB–2): (**a**) EL Centro; (**b**) Taft; (**c**) Chi–Chi; (**d**) Kobe.

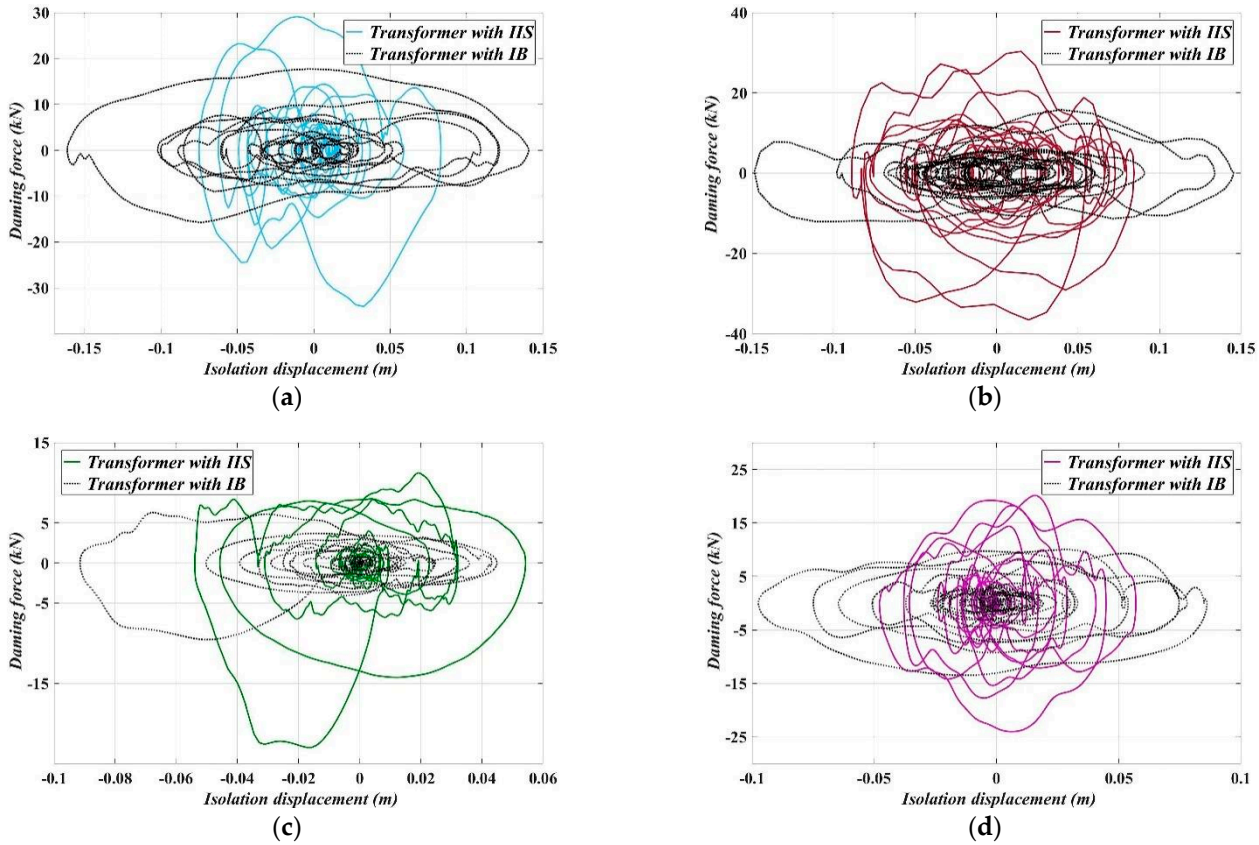

Figure 18. Hysteresis loops of isolation layer (LB–2): (**a**) EL Centro; (**b**) Taft; (**c**) Chi–Chi; (**d**) Kobe.

The isolation system with inerter element increases the mass effect and viscous damping effect of the isolation layer, but it does not mean that the system needs greater apparent mass and damping coefficient. On the contrary, the inerter system can change the original small apparent mass into a larger equivalent mass (such as moment of inertia), which can be dozens or even hundreds of times the original mass, so as to reduce the actual mass and volume of the isolation layer. However, the natural period of the superstructure can still be extended, and the displacement of the isolation layer can be reduced under the condition of ensuring the isolation rate. This has high practical value for engineering.

5. Conclusions

In this paper, the influence of the inerter isolation system (IIS) on the response of the transformer–bushing system was studied, and the parameter optimization design of IIS was carried out. Finally, the isolation performance of IIS under different input was analyzed. The main conclusions are as follows:

1. The equivalent mass coefficient and damping coefficient of IIS can be amplified by an inerter element, and the inerter–mass ratio and damping ratio are reduced simultaneously under the condition of meeting the performance demand after parameter optimization.
2. The proposed optimal design utilizes the most efficient parameter set of inerter–mass ratio and damping ratio for the relative displacement ratio of the bushing and tank in the extremum condition. The parameter optimization design method proved to be effective in meeting the target demand of relative displacement response of the bushing and tank, while base shear force and isolation displacement were reduced simultaneously.
3. Based on results from response history analysis under ground motion records, IIS can significantly suppress the resonance response of the structure and the continuous vibration response in the stable state and its peak displacement can be reduced by 50% compared with IB. IIS has a smaller displacement of the isolation layer than IB, and the peak displacement is about 45–60% of IB.

In conclusion, IIS has considerable vibration mitigation effect. This study mainly focuses on the macro–structural design parameters of typical transformer–bushing systems, but there is no detailed analysis on the design parameters of any specific IIS device. At present, the IIS device is in the development stage. Subsequent research will carry out mechanical performance tests according to the specific device with inerter, damper, and spring. More combinations of isolation system with inerter and parameters optimization methods will also be discussed. Furthermore, a shaking table test will be carried out on the specific structure with IIS installed.

Author Contributions: R.Z.: Methodology, Conceptualization, Software, Investigation, Writing—original draft, Writing—review & editing; M.C.: Conceptualization, Supervision, Funding acquisition, Writing—review & editing; J.H.: Validation, Writing—review & editing. All authors have read and agreed to the published version of the manuscript.

Funding: This research was supported by 2020 open fund project of the State Key Laboratory of Disaster Prevention & Reduction for Power Grid Transmission and Distribution Equipment (B316AF190007) and State Grid Science & Technology Project (5200-201919121A-0-0-00).

Institutional Review Board Statement: Not applicable.

Informed Consent Statement: Not applicable.

Data Availability Statement: The data used to support the findings of this study are included within the article.

Conflicts of Interest: The authors declare that there is no conflict of interest regarding the publication of this paper. The authors declare no conflict of interest.

References

1. Meigen, C.; Fulin, Z.; Ping, P.; Guangping, Z.; Zhengguo, G. Seismic response of transformer and bushing isolation system and parameter analysis of isolation layer. *Proc. CSEE* **2012**, *32*, 166–174.
2. Li, T.; Hai–Yang, P.; Rui–Sheng, M. Probabilistic seismic demand model and fragility analysis of transmission tower subjected to near–field ground motions. *J. Constr. Steel Res.* **2019**, *156*, 266–275.
3. Meirovitch, L. *Dynamics and Control of Structures*; John Wiley & Sons: New York, NY, USA, 1990.
4. Soong, T.T.; Dargush, G.F. *Passive Energy Dissipation Systems in Structural Engineering*; Wiley: Chichester, UK, 1997.
5. Cao, M.; Fan, R.; Li, S.; Cao, C.; Lu, Z.; Zhang, X. Design and application of seismic isolation system of large power transformer and bushings system. *Power Syst. Technol.* **2011**, *35*, 130–135.
6. Fujita, T.; Fujita, S.; Yoshizawa, T.; Suzuki, S. Base Isolation Support of Heavy Equipment with Laminated Rubber Bearings–2. *Jpn. Soc. Mech. Eng.* **1985**, *51*, 461.
7. Bonacina, G.; Bonetti, P.; Martelli, A.; Bettinali, F.; Serino, G. Seismic base isolation of gas insulated electrical substations: Design, experimental and numerical activities, evaluation of the applicability. In Proceedings of the 10th European Conference on Earthquake Engineering, Vienna, Austria, 28 August–2 September 1995.
8. Pham, T. *Two–Dimensional Shaking Table Test of Transformer Bushing with Seismic Isolation Device*; MCEER Report; Department of Civil and Environmental Engineering, University of California at Irvin: Irvine, CA, USA, 2005.
9. Murota, N.; Feng, M.Q.; Liu, G.Y. Earthquake Simulator Testing of Base–Isolated Power Transformers. *IEEE Trans Power Deliv* **2006**, *21*, 1291–1299. [CrossRef]
10. Murota, N.; Feng, M.Q.; Liu, G.Y. *Experimental and Analytical Studies of Base Isolation Systems for Seismic Protection of Power Transformers*; Technical Report MCEER-05-0008; Multidisciplinary Center for Earthquake Engineering Research: Buffalo, NY, USA, 2005.
11. Jiyu, L.; Junxiong, L.; Ruimin, L.; Peimin, L. Experiment and system identification of base–isolated electric power transformer. *Earthq. Eng. Eng. Vib.* **2001**, 109–116.
12. Lee, S.H.; Min, K.W.; Hwang, J.S.; Kim, J. Evaluation of equivalent damping ratio of a structure with added dampers. *Eng. Struct.* **2004**, *26*, 335–346. [CrossRef]
13. Smith, M.C.; Wang, F.C. Performance benefits in passive vehicle suspensions employing inerters. *Veh. Syst. Dyn.* **2004**, *42*, 235–257. [CrossRef]
14. Smith, M.C. Synthesis of mechanical networks: The inerter. *IEEE Trans. Autom. Control* **2002**, *47*, 1648–1662. [CrossRef]
15. Swift, S.J.; Smith, M.C.; Glover, A.R.; Papageorgiou, C.; Gartner, B.; Houghton, N.E. Design and modelling of a fluid inerter. *Int. J. Control* **2013**, *86*, 2035–2051. [CrossRef]
16. Ikago, K.; Saito, K.; Inoue, N. Seismic control of single–degree–of–freedom structure using tuned viscous mass damper. *Earthq. Eng. Struct. Dyn.* **2012**, *41*, 453–474. [CrossRef]
17. Pan, C.; Zhang, R. Design of structure with inerter system based on stochastic response mitigation ratio. *Struct. Control Health Monit.* **2018**, *25*, e2169. [CrossRef]
18. Pan, C.; Zhang, R.; Luo, H.; Li, C.; Shen, H. Demand–based optimal design of oscillator with parallel–layout viscous inerter damper. *Struct. Control Health Monit.* **2018**, *25*, e2051. [CrossRef]
19. Hwang, J.S.; Kim, J.; Kim, Y.M. Rotational inertia dampers with toggle bracing for vibration control of a building structure. *Eng. Struct.* **2007**, *29*, 1201–1208. [CrossRef]
20. Zhang, R.F.; Zhao, Z.P.; Dai, K.S. Seismic response mitigation of a wind turbine tower using a tuned parallel inerter mass system. *Eng. Struct.* **2019**, *180*, 29–39. [CrossRef]
21. Zhao, Z.P.; Zhang, R.F.; Wierschem, N.E.; Jiang, Y.Y.; Pan, C. Displacement mitigationoriented design and mechanism for inerter–based isolation system. *J. Vib. Control* **2020**, *27*, 1991–2003. [CrossRef]
22. Gao, H.; Wang, H.; Li, J.; Wang, Z.; Liang, R.; Xu, Z.; Ni, Y. Optimum design of viscous inerter damper targeting multi–mode vibration mitigation of stay cables. *Eng. Struct.* **2021**, *226*, 111375. [CrossRef]
23. Sugimura, Y.; Goto, W.; Tanizawa, H.; Saito, K.; Nimomiya, T. Response control effect of steel building structure using tuned viscous mass damper. In Proceedings of the 15th World Conference on Earthquake Engineering, Lisbon, Portugal, 25–28 September 2012.
24. Kurata, M.; Leon, R.T.; Desroches, R. Rapid seismic rehabilitation strategy: Concept and testing of cable bracing with couples resisting damper. *J. Struct. Eng.* **2012**, *138*, 354–362. [CrossRef]
25. Xie, L.; Ban, X.; Xue, S.; Ikago, K.; Kang, J.; Tang, H. Theoretical Study on a Cable–Bracing Inerter System for Seismic Mitigation. *Appl. Sci.* **2019**, *9*, 4096. [CrossRef]
26. Xue, S.; Kang, J.; Xie, L.; Zhang, R.; Ban, X. Cross–Layer Installed Cable–Bracing Inerter System for MDOF Structure Seismic Response Control. *Appl. Sci.* **2020**, *10*, 5914. [CrossRef]
27. Wang, H.; Gao, H.; Li, J.; Wang, Z.; Ni, Y.; Liang, R. Optimum design and performance evaluation of the tuned inerter–negative–stiffness damper for seismic protection of single–degree–of–freedom structures. *Int. J. Mech. Sci.* **2021**, *212*, 106805. [CrossRef]
28. Luo, H.; Zhang, R.F.; Weng, D.G. Mitigation of liquid sloshing in storage tanks by using a hybrid control method. *Soil Dyn. Earthq. Eng.* **2016**, *90*, 183–195. [CrossRef]
29. Jiang, Y.Y.; Zhao, Z.P.; Zhang, R.F.; De Domenico, D.; Pan, C. Optimal design based on analytical solution for storage tank with inerter isolation system. *Soil Dyn. Earthq. Eng.* **2020**, *129*, 105924. [CrossRef]

30. Losanno, D.; Calabrese, A.; Madera–Sierra, I.E.; Spizzuaco, M.; Marulanda, J.; Thomson, P.; Serino, G. Recycled versus Natural–Rubber Fiber–Reinforced Bearings for Base Isolation: Review of the Experimental Findings. *J. Earthq. Eng.* **2022**, *26*, 1921–1940. [CrossRef]
31. Losanno, D.; Palumbo, F.; Calabrese, A.; Barrasso, T.; Vaiana, N. Preliminary Investigation of Aging Effects on Recycled Rubber Fiber Reinforced Bearings (RR–FRBs). *J. Earthq. Eng.* **2021**, 1–18. [CrossRef]
32. Kelly, J.M. Seismic isolation for earthquake–resistant design. In *Earthquake–Resistant Design with Rubber*; Springer: London, UK, 1997; pp. 1–18.
33. Vaiana, N.; Spizzuoco, M.; Serino, G. Wire rope isolators for seismically base–isolated lightweight structures: Experimental characterization and mathematical modeling. *Eng. Struct.* **2017**, *140*, 498–514. [CrossRef]
34. Nagarajaiah, S.; Reinhorn, A.M.; Constantinou, M.C. Nonlinear Dynamic Analysis of 3–D–Base–Isolated Structures. *J. Struct. Eng.* **1991**, *117*, 2035–2054. [CrossRef]
35. Pellecchia, D.; Feudo, S.L.; Vaiana, N.; Dion, J.L.; Rosati, L. A procedure to model and design elastomeric–based isolation systems for the seismic protection of rocking art objects. *Comput.-Aided Civ. Infrastruct. Eng.* **2021**. [CrossRef]